AIAA JOURNAL
Vol. 31, No. 11, November 1993

Analysis of High Reynolds Number Inviscid/Viscid Interactions in Cascades

M. Barnett,* J. M. Verdon,† and T. C. Ayer‡
United Technologies Research Center, East Hartford, Connecticut 06108

An efficient analysis for predicting steady, strong, inviscid/viscid interaction phenomena, such as viscous-layer separation, shock/boundary-layer interaction, and trailing-edge/near-wake interaction, in turbomachinery blade passages is needed as part of a comprehensive analytical blade design prediction system. Such an analysis is described in the present paper. It uses an inviscid/viscid interaction approach, in which the flow in the outer inviscid region is assumed to be potential and the flow in the inner or viscous-layer region is governed by Prandtl's equations. The inviscid solution is determined using an implicit, least-squares, finite difference approximation; the viscous-layer solution is determined using an inverse, finite difference, space-marching method, which is applied along the blade surfaces and wake streamlines. The inviscid and viscid solutions are coupled using a semi-inverse global iteration procedure, which permits the prediction of boundary-layer separation and other strong-interaction phenomena. Results are presented for two cascades, with a range of inlet flow conditions considered for one of them, including conditions leading to large-scale flow separations. Comparisons with Navier-Stokes solutions are also given.

Introduction

An important problem faced by engine designers is the prediction of high Reynolds number (Re) viscous flow and, in particular, viscous separation phenomena in compressor and turbine blade passages. Viscous effects control aerodynamic losses, heat transfer rates, and stall and hence must be accounted for. In addition to performance characteristics, the ability to account for unsteady viscous effects is needed for aeroelastic and aeroacoustic design applications, e.g., to predict the onset of stall flutter, blade row interactions due to the convection of viscous wakes from upstream rows, and other unsteady effects that impact the structural and acoustic characteristics of turbomachinery blade rows. Clearly, efficient analytical procedures for predicting steady and unsteady viscous flows in high-performance blading would be a significant contribution to a successful blade design prediction system.

The analysis described in this paper is being developed as part of a research program to construct reliable and efficient theoretical prediction methods for steady and unsteady viscous flows through subsonic and transonic cascades. The approach to be followed is similar to that which has been applied successfully in external aerodynamics, where inviscid/viscid interaction (IVI) concepts have been used to predict steady[1,2] and unsteady[3,4] flowfields.

The construction of an IVI procedure for cascades involves, first, the development of component (i.e., inviscid and viscous) flow solvers and, second, the implementation of these component solvers into a strong-interaction computational procedure to produce a complete viscous analysis. Solution methods for steady subsonic and transonic inviscid flows through cascades and for steady boundary-layer and wake flows have been developed to a relatively mature state. Methods for coupling such solutions have also been developed and assessed through a number of model problem studies (e.g., see Refs. 5 and 6). Inviscid/viscid interaction procedures for predicting steady flow in cascades have also been developed[7-9] and applied over a wide range of inlet flow conditions, including conditions leading to stall.[9]

The focus of this paper is on the development of an accurate and efficient steady cascade analysis that will provide the foundation for an unsteady procedure to be developed later. In the present approach, the "outer" inviscid flow is determined using the steady, full-potential analysis (SFLOW) developed by Hoyniak and Verdon.[10] In the overall calculation procedure (which will be referred to as SFLOW-IVI), viscous effects are incorporated by adjusting the blade and wake surface boundary conditions in SFLOW to account for the effects of viscous displacement. The nonlinear inviscid analysis, coupled with the IVI iteration procedure, allows nonlinear changes to the base flow to be evaluated. The ability to treat nonlinear perturbations is especially important in transonic flows in which shock positions are significantly altered by viscous displacement effects. Although the analysis described in this paper is currently restricted to subsonic flows, it will be extended to treat transonic flows in the future.

General Concepts

For the flows of practical interest in either external or internal aerodynamics, the Reynolds number is usually sufficiently high so that the flow past an airfoil or blade can be divided into two regions: an "inner" dissipative region consisting of boundary layers and wakes and an "outer" inviscid region. The principal interaction between the flows in the viscid and inviscid regions arises from the displacement thickness effect that leads to thickened semi-infinite equivalent bodies with corresponding changes in surface pressures. If the interaction is "weak," then the complete flow problem can be solved sequentially. Flows over airfoils, however, involve both a weak overall interaction, arising from standard displacement thickness and wake curvature effects, and local strong-displacement interactions caused, for example, by viscous-layer separations, shock/boundary-layer interactions, and trailing-edge/near-wake interactions. Viscous displacements in strong-interaction regions cause substantial changes in the local inviscid pressure fields and can, in some cases (e.g., in flows with large-scale separations), cause substantial changes in the global pressure field. The concept of an inner viscous region and an outer inviscid region still holds, but the classical hierar-

Presented as Paper 92-3073 at the AIAA/SAE/ASME/ASEE 28th Joint Propulsion Conference, Nashville, TN, July 6-8, 1992; received Sept. 4, 1992; revision received Jan. 27, 1993; accepted for publication Jan. 30, 1993.

*Senior Research Engineer, Theoretical & Computational Fluid Dynamics. Senior Member AIAA.

†Manager, Theoretical and Computational Fluid Dynamics. Associate Fellow AIAA.

‡Assistant Research Engineer, Theoretical & Computational Fluid Dynamics. Member AIAA.

chical structure of the flow no longer applies. Thus, in a local strong-interaction region, the hierarchy changes from "direct" (i.e., pressure determined by the inviscid flow) to "interactive" (i.e., pressure determined by a mutual interaction between the inviscid and the viscous-layer flows), and this change must be accommodated within an inviscid/viscid interaction solution procedure.

The approach taken here employs an IVI model to calculate high Reynolds number flows through two-dimensional cascades. The nonhierarchical nature of strong interactions is accounted for in the global iteration procedure used to couple the inviscid and viscous solutions. In addition, an *inverse* viscous-layer calculation, in which the displacement thickness is specified instead of the pressure, is employed to permit viscous solutions to be continued through local strong-interaction regions, including regions of separated flow. In regions of the flow where the viscous layer remains attached, the pressure, as determined from the inviscid solution, can be imposed instead of the displacement thickness. This latter or "classical" approach is known as a *direct* viscous-layer procedure.

We consider high Reynolds number ($Re = \rho^*_{-\infty} V^*_{-\infty} L^* / \mu^*_{-\infty}$) steady flow, with negligible body forces, of a perfect gas with constant specific heats and Prandtl number through a two-dimensional cascade, as shown in Fig. 1. In the following discussion, all flow variables and spatial coordinates are dimensionless. Lengths have been scaled with respect to the blade chord (L^*); density, velocity, and viscosity with respect to their inlet freestream values ($\rho^*_{-\infty}$, $V^*_{-\infty}$, and $\mu^*_{-\infty}$, respectively); pressure with respect to twice the inlet freestream dynamic pressure ($\rho^*_{-\infty} V^{*2}_{-\infty}$); and temperature with respect to the square of the inlet freestream speed divided by the specific heat at constant pressure ($V^{*2}_{-\infty}/c^*_p$). Here the superscript * denotes a dimensional quantity and the subscript $-\infty$ refers to the prescribed freestream conditions far upstream.

Inviscid Region

The subsonic inviscid flow is assumed to be isentropic and irrotational; hence, a velocity potential Φ exists and is governed by the field equation

$$A^2 \nabla^2 \Phi = \nabla\Phi \cdot \nabla(\nabla\Phi)^2/2 \tag{1}$$

The speed of sound propagation A, the fluid pressure P, density ρ, and temperature T are related through Bernoulli's equation and the isentropic relations as follows:

$$(M_{-\infty}A)^2 = (\gamma M^2_{-\infty} P)^{(\gamma-1)/\gamma} = \rho^{(\gamma-1)}$$

$$= (\gamma - 1) M^2_{-\infty} T = 1 - [(\gamma - 1)/2] M^2_{-\infty} [(\nabla\Phi)^2 - 1] \tag{2}$$

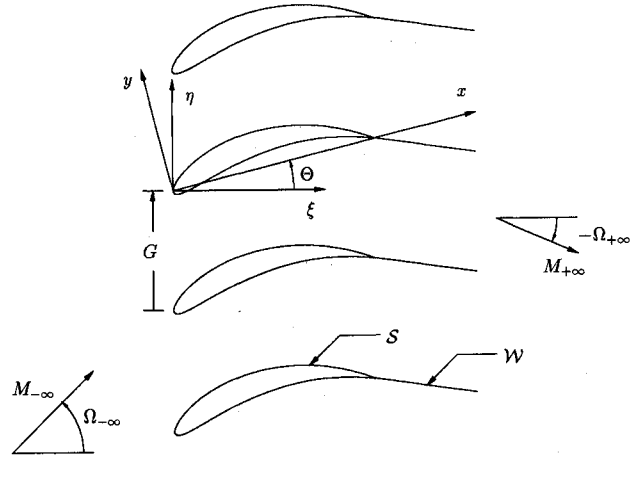

Fig. 1 Two-dimensional compressor cascade.

where M is the Mach number and γ is the specific heat ratio of the fluid. The inviscid flow is determined as a solution of Eq. (1) subject to a flow tangency condition at each blade surface, cascade periodicity conditions upstream and downstream of the blade row, jump conditions on normal velocity and pressure across blade wakes, and appropriate uniform flow conditions far upstream of the blade row. A Kutta condition is applied at blade trailing edges in lieu of specifying the exit flow angle. Finally, far downstream of the blade row, global mass conservation is enforced, accounting for blockage effects due to the viscous layers.

The specific forms of the blade and wake conditions follow from an asymptotic matching of the outer inviscid and the inner viscous-layer equations.[1] Thus, the inviscid solution for the normal velocity at a blade surface must match the viscous solution for this velocity at the outer edge of the viscous layer. It follows, after carrying out the asymptotic matching, that

$$\nabla\Phi \cdot \boldsymbol{n}\,|_{\mathcal{S}} = \rho_e^{-1} \frac{\mathrm{d}(\rho_e u_e \delta)}{\mathrm{d}s} \tag{3}$$

where $\mathcal{S}$ denotes a reference blade surface (see Fig. 1), ρ_e and u_e are the inviscid density and velocity at this surface (or the viscous density and streamwise velocity component at the edge of the viscous layer), and δ is the boundary-layer displacement thickness. The quantities s and $\boldsymbol{n}$ denote the arc distance along the blade (positive in the downstream direction and zero at the leading-edge stagnation point) and the local unit normal vector directed outward from the surface, respectively.

Two types of terms arise from the wake-matching conditions, one due to the wake viscous displacement and the other due to the wake curvature. The first leads to the requirement that the inviscid solution for the normal component of velocity must be discontinuous with jump given by

$$[\![\nabla\Phi]\!] \cdot \boldsymbol{n}\,|_{\mathcal{W}} = \rho_e^{-1} \frac{\mathrm{d}(\rho_e u_e \delta_{\mathcal{W}})}{\mathrm{d}s} \tag{4}$$

where $[\![\,]\!]$ denotes the difference in a quantity (upper minus lower) across the wake, $\boldsymbol{n}$ is the upward pointing unit normal vector to the reference wake streamline (i.e., $\mathcal{W}$ in Fig. 1), and $\delta_{\mathcal{W}}$ is the displacement thickness of the complete wake. The wake curvature effect gives rise to a static pressure difference across the wake. The requirement that the outer inviscid flow should match this pressure difference leads to the condition

$$[\![P]\!]_{\mathcal{W}} = \kappa \rho_e u_e^2 (\delta_{\mathcal{W}} + \theta_{\mathcal{W}}) \tag{5}$$

where $\theta_{\mathcal{W}}$ is the momentum thickness of the complete wake and κ is the curvature of the wake that is taken as positive when the reference wake streamline is concave upwards.

A complication arises in that the location of the reference wake streamline is unknown a priori; however, to within lowest order, the wake conditions can be referenced to any arbitrary curve emanating from the trailing edge and lying within the actual viscous wake.[6] In the present study, the reference wake streamline is taken to be the aft stagnation streamline as determined from the pure inviscid solution.

After quasilinearizing the nonlinear terms, the full-potential equation is discretized and solved using an implicit, least-squares, finite-difference approximation. The resulting matrix system of algebraic difference equations is inverted directly using lower-upper decomposition and Gaussian elimination. A fixed-point iteration method is used to update the nonlinear inviscid solution. This analysis, called SFLOW, is described in more detail in Ref. 10. Present inviscid solutions were obtained on a "streamline" type H-mesh rather than on the "sheared" H-mesh of Ref. 10. The SFLOW analysis was modified by Hoyniak[11] to use the streamline H-mesh developed by Verdon and Hall.[12] Thus, before starting an IVI calculation, an inviscid solution is obtained on a sheared H-mesh. The resulting solution is then used to generate a stream-

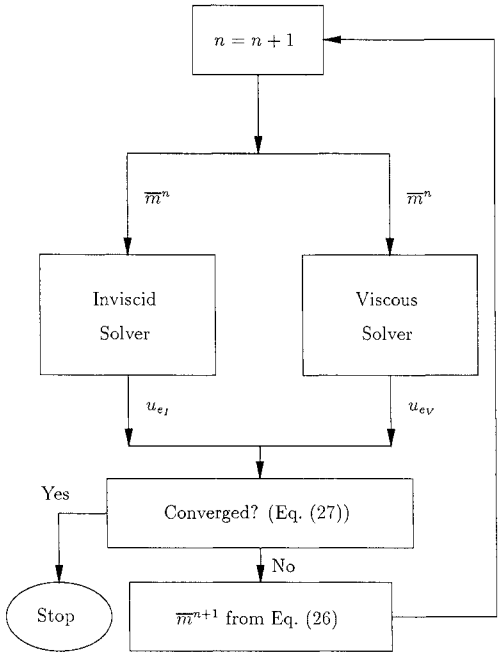

Fig. 2 Semi-inverse iteration procedure.

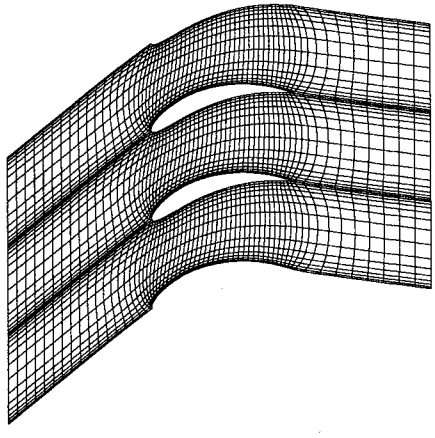

Fig. 3 Streamline H-mesh for the EGV cascade.

line H-mesh, in which one set of mesh lines corresponds to the streamlines of the inviscid flow, and the second family consists of lines that are "nearly" orthogonal to the first set. The principal advantage of the streamline H-mesh over the sheared mesh is an improved resolution of the flow near blade leading edges.

Viscous Layer

The flow in the inner or viscous region is assumed to be governed by Prandtl's viscous-layer equations. After introducing the scaled normal coordinate $\tilde{n} = Re^{1/2}n$ and normal velocity component $\tilde{v} = Re^{1/2}v$, the continuity and streamwise momentum equations have the form

$$\frac{\partial(\rho u)}{\partial s} + \frac{\partial(\rho \tilde{v})}{\partial \tilde{n}} = 0 \tag{6}$$

and

$$\rho\left(u\frac{\partial u}{\partial s} + \tilde{v}\frac{\partial \tilde{v}}{\partial \tilde{n}}\right) - \rho_e u_e \frac{\mathrm{d}u_e}{\mathrm{d}s} = \frac{\partial}{\partial \tilde{n}}\left(\mu_T \frac{\partial u}{\partial \tilde{n}}\right) \tag{7}$$

where u is the velocity component along the blade or reference wake streamline and $u > 0$ when the flow is in the direction of increasing s. Here we assume that the flow in the viscous layer is adiabatic at unit Prandtl number; thus, the energy equation reduces to the requirement that the total enthalpy of the fluid $H = T + u^2/2$ must be constant across the viscous layer. In Eq. (7) the subscript e refers to fluid properties at the edge of the viscous layer, and $\mu_T = \mu + \gamma_T e$ is the effective turbulent viscosity, where e is the turbulent eddy viscosity, γ_T is the longitudinal intermittency factor, and μ is the molecular viscosity, which is assumed to be a function of temperature alone. The eddy-viscosity model employed in the present analysis for blade surface boundary layers is the model of Cebeci and Smith,[13] modified to account for separated flow[5]; in the wake, the model of Chang et al.[14] is used. The locations at which instantaneous transition occurs are specified by the user.

The foregoing field equations govern the flow in the viscous layers along the upper and lower surfaces of the blades and in the blade wakes. They are solved subject to conditions at the edges of the viscous layers, at the blade surfaces, and along the reference wake streamlines, i.e.,

$$u \to u_e \quad \text{for} \quad \tilde{n} \to \infty, \quad s \geq 0 \tag{8}$$

$$u = \tilde{v} = 0 \quad \text{for} \quad \tilde{n} = 0, \quad 0 \leq s \leq s_{TE}^{\pm} \tag{9}$$

and

$$\tilde{v} = 0 \quad \text{for} \quad \tilde{n} = 0, \quad s > s_{TE}^{\pm} \tag{10}$$

respectively, where $s_{TE}^{\pm}$ are the trailing-edge values of the upper- (+) and lower-surface (−) arc-length coordinates measured from the leading-edge stagnation point. The condition expressed by Eq. (8) is also applied along the wake streamline for $\tilde{n} \to -\infty$. Equations (9) and (10) imply that the curve $\tilde{n} = 0$ corresponds to the blade surfaces and reference wake streamlines, respectively.

The displacement δ and momentum θ thicknesses of the viscous layers are needed to determine the effect of viscous displacement and wake curvature on the outer inviscid flow [cf. Eqs. (3-5)]. They are defined by

$$\delta(s) = Re^{-1/2}\int_0^{\infty}\left(1 - \frac{\rho u}{\rho_e u_e}\right)\mathrm{d}\tilde{n} \tag{11}$$

and

$$\theta(s) = Re^{-1/2}\int_0^{\infty}\frac{\rho u}{\rho_e u_e}\left(1 - \frac{u}{u_e}\right)\mathrm{d}\tilde{n} \tag{12}$$

where the zero lower bound on the integrals is replaced with $-\infty$ for $s >$ for $s_{TE}^{\pm}$.

The independent and dependent variables appearing in the viscous-layer equations are transformed using a modified form[5] of the Levy-Lees transformation.[15] Thus, the independent variables are given by

$$\xi = \int_0^s \rho_e u_e \mu_e e_o \,\mathrm{d}s \quad \text{and} \quad \eta = \rho_e u_e (2\xi)^{-1/2}\int_0^{\tilde{n}} \rho/\rho_e \,\mathrm{d}\tilde{n} \tag{13}$$

and the dependent variables are defined by

$$F = u/u_e \quad \text{and} \quad f = (2\xi)^{-1/2}\psi \tag{14}$$

The quantity $e_o(s)$ is the value of the eddy viscosity in the outer region of the viscous layer, as defined in the Cebeci-Smith[13] model. It appears in the definition of ξ to maintain a nearly constant η value at the edge of a turbulent boundary layer.[16] The Levy-Lees transformation permits the leading-edge stagnation-point similarity solution to be recovered and reduces the truncation error of the viscous solution over that

associated with the use of primitive variables. The quantity ψ is the compressible stream function, defined in terms of the velocity components u and $\bar{v}$, from the relations $\rho u = \partial\psi/\partial\bar{n}$ and $\rho\bar{v} = -\partial\psi/\partial s$.

The continuity and momentum equations transform to

$$F = \frac{\partial f}{\partial \eta} \tag{15}$$

and

$$\frac{\partial}{\partial\eta}\left(\ell\bar{\epsilon}\frac{\partial f}{\partial\eta}\right) - 2\xi F\frac{\partial F}{\partial\xi} + \left(f + 2\xi\frac{\partial f}{\partial\xi}\right)\frac{\partial F}{\partial\eta} + (\hat{\theta} - F^2)\beta = 0 \tag{16}$$

where $\ell = \rho\mu/\rho_e\mu_e$, $\bar{\epsilon} = \mu_t/\mu$, and β is a pressure gradient parameter defined by

$$\beta = \frac{2\xi}{u_e}\frac{du_e}{d\xi} \tag{17}$$

The quantity $\hat{\theta} = T/T_e$ is the local-to-edge static temperature ratio and is related to F by

$$\hat{\theta} = 1 + \frac{\gamma - 1}{2}M_e^2(1 - F^2) \tag{18}$$

The molecular viscosity coefficient μ is determined using the Sutherland viscosity law.

The following boundary conditions are applied. The stream function is constant along blade and reference wake streamlines ($\eta = 0$), and, without loss in generality, we can set

$$f = 0 \quad \text{at} \quad \eta = 0 \tag{19}$$

The no-slip condition applies at a blade surface, i.e.,

$$F = 0 \quad \text{at} \quad \eta = 0, \quad \xi \le \xi_{TE} \tag{20}$$

where ξ_{TE} is the trailing-edge value of ξ. At the edges of the surface viscous layers $F(\eta_e) = 1$ since $u \to u_e$ as $\eta \to \eta_e$. The wake boundary conditions for F are more complicated because of the pressure jump [cf. Eq. (5)]. In the wake we denote the upper- and lower-edge values of η by η_e^+ and η_e^-, respectively, and the corresponding values of u_e by the appropriate $\pm$ superscript. Letting $F = u/u_e^+$, the boundary condition at η_e^+ is $F(\eta_e^+) = 1$. The boundary condition at η_e^- is obtained from Eq. (5) and Bernoulli's equation. The result is

$$\tfrac{1}{2}\rho_e^+ u_e^{+2}\left[\frac{\rho_e^-}{\rho_e^+}\left(\frac{u_e^-}{u_e^+}\right)^2 - 1\right] = \kappa(\rho_e u_e^2)_{\text{avg}}(\delta + \theta)_W \tag{21}$$

where $(\rho_e u_e^2)_{\text{avg}} = (\rho_e^+ u_e^{+2} + \rho_e^- u_e^{-2})/2$. Using Eq. (2), ρ can be eliminated in favor of u by invoking the assumption that $u_e \gg v_e$ (consistent with boundary-layer theory), i.e., $(\nabla\Phi)^2 \approx u^2$. The result is a nonlinear equation relating $F(\eta_e^-) = u_e^-/u_e^+$ and the right-hand side of Eq. (21). If the curvature effect is negligible, i.e., $[\![P]\!]_W \approx 0$, the latter boundary condition becomes $F(\eta_e^-) = 1$.

The viscous-layer equations are parabolic in the ξ direction and therefore require initial conditions. These are provided by a similarity solution at the leading-edge stagnation point $\xi = 0$, which is obtained by solving the viscous equations for $\beta = 1$. The blade and wake solutions are then determined by space marching in the downstream direction. The equations are solved in the direct mode (i.e., β specified) near the leading edge and in the inverse mode (i.e., δ specified) downstream of an axial station whose location is either prescribed in advance or determined during the calculation to ensure that the inverse mode is initiated upstream of a separation point. The wake is calculated using the inverse mode.

In the direct viscous-layer calculation, the value of β is determined by the inviscid analysis, and the displacement thickness is obtained from the viscous analysis. In the inverse procedure, the displacement thickness is specified, and the edge values of the variables β, u_e, etc., are obtained as part of the viscous-layer solution. This is accomplished by introducing a "mass deficit parameter," $\overline{m} = \rho_e u_e \delta$. An expression relating the value of f at the edge of the viscous layer to $\overline{m}$, i.e.,

$$f(\eta_e) = h + \eta_e - (\overline{m}/\sqrt{2\xi}) \tag{22}$$

where

$$h = \int_0^{\eta_e} (\hat{\theta} - 1)\, d\eta \tag{23}$$

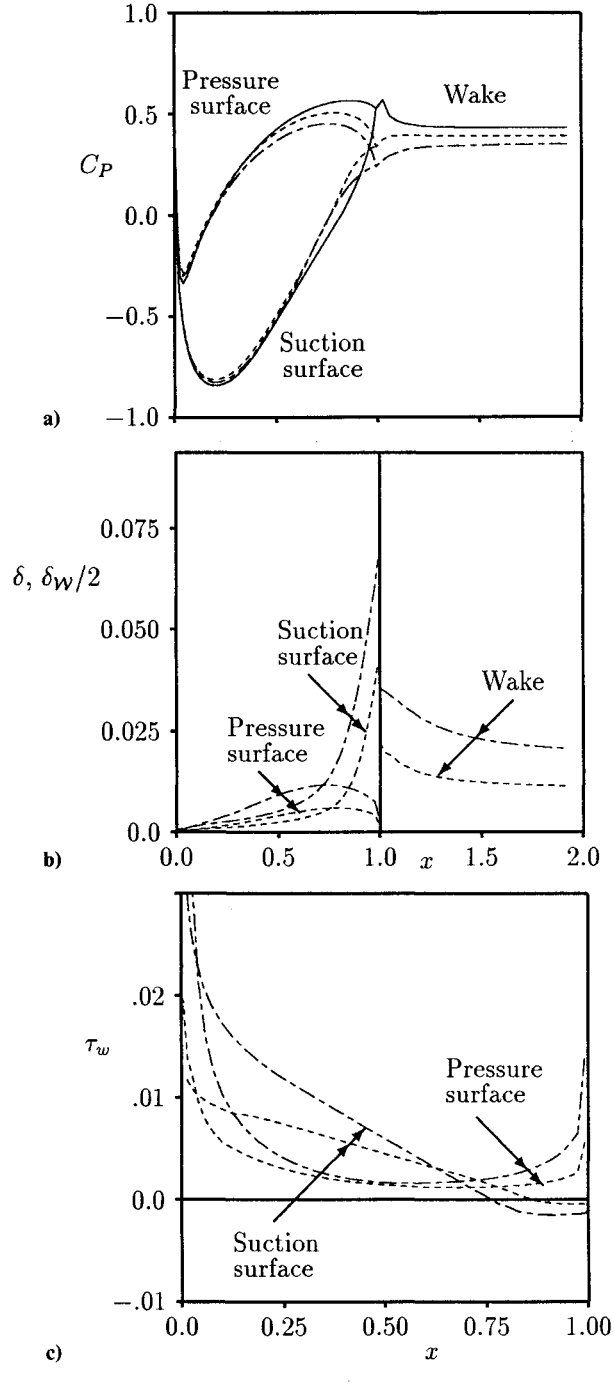

Fig. 4 Inviscid (——) and IVI solutions for EGV cascade at $Re = 10^5$ (— — — —) and 10^6 (- - - - -): a) pressure coefficient, b) displacement thickness, and c) surface shear stress.

is derived by integrating Eq. (15) across the layer and employing the definition of δ [Eq. (11)]. The parameter h is specified and is lagged from the previous global IVI iteration. Similarly, in the wake an expression for the *jump* in the stream function between the viscous-layer upper and lower edges is derived by integrating Eq. (15) across the entire wake (from η_e^- to η_e^+) and using the definition of the displacement thickness, i.e.,

$$f(\eta_e^+) - f(\eta_e^-) = h_{\mathcal{W}} + \eta_e^+ - \eta_e^- - (\overline{m}_{\mathcal{W}}/\sqrt{2\xi}) \qquad (24)$$

where

$$h_{\mathcal{W}} = \int_{\eta_e^-}^{\eta_e^+} (\hat{\theta} - 1)\, d\eta \qquad (25)$$

Equations (24) and (25) are used to impose $\overline{m}_{\mathcal{W}} = (\rho_e u_e \delta)_{\mathcal{W}}$ and $h_{\mathcal{W}}$ in the same way that the corresponding equations were used on the blade surfaces to impose $\overline{m}$ and h. In the inverse mode the quantities β and u_e are unknown. Thus, a supplemental equation relating these two variables is needed. This relation is obtained by discretizing Eq. (17), which defines β in terms of u_e.

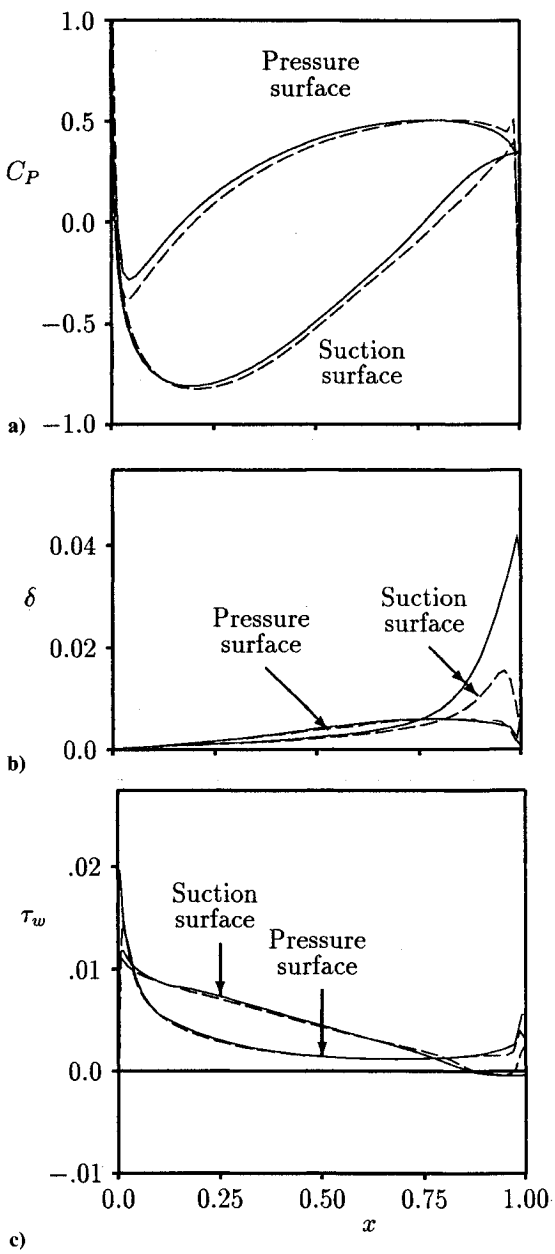

Fig. 5 Comparison of IVI (——) and Navier-Stokes (- - - - -) solutions for the EGV cascade at $Re = 10^6$: a) pressure coefficient, b) displacement thickness, and c) surface shear stress.

The discretized field equations, boundary conditions, and auxiliary conditions, Eqs. (15–25), are quasilinearized, and the resulting tridiagonal system of algebraic equations is solved at each s station, using a fixed-point iteration to update the nonlinear terms. The inversion algorithm used in the wake is modified to account for the application of one boundary condition [Eq. (19)] at $\eta = 0$ and the others at the upper and lower edges of the viscous layer, as well as to account for the application of a jump condition on f [Eq. (24)] between the upper and lower edges. Finally, the so-called FLARE approximation, which prevents instabilities in the viscous-layer solution due to axial flow reversal, is applied by turning off all of the convective terms in the momentum equation wherever $F < 0$. Further details on the viscous-layer numerical analysis can be found in Ref. 17.

Inviscid/Viscid Interaction

The IVI approach used here determines the complete flowfield by iteratively updating the mass deficit parameter $\overline{m}(s)$, which affects the inviscid and viscous solutions through their respective boundary conditions. For an arbitrary $\overline{m}$ distribution, two different surface and wake streamline velocity distributions generally result: one, $u_{e_I}(s)$, from the inviscid calculation and one, $u_{e_V}(s)$, from the viscous-layer calculation. The objective is to determine a converged inviscid/viscid interaction solution by finding the mass deficit parameter distribution that reduces the difference between the u_{e_I} and u_{e_V} distributions to an acceptably low level, as defined later.

In this investigation, the "semi-inverse" iteration procedure of Carter[18] is used to update $\overline{m}$ at every streamwise mesh station on the blade and wake surfaces. Thus, we set

$$\overline{m}^{n+1} = \overline{m}^n [1 + \omega(u_{e_V}^n / u_{e_I}^n - 1)] \qquad (26)$$

where the superscript n is the global iteration count and ω is a relaxation parameter. The solution is considered to be converged when

$$\max_i |u_{eV_i} - u_{e_{I_i}}| / u_{e_{I_i}} < \hat{\epsilon}, \qquad i = 1, \ldots, IE \qquad (27)$$

where the value of $\hat{\epsilon}$ is specified by the user and IE is the number of streamwise mesh stations. Equation (27) is applied on both blade surfaces and along the wake. The viscous-layer solution is obtained at the locations corresponding to the intersections of the inviscid mesh with the blade and wake streamlines, which avoids the need for interpolation. During the global iterations, the independent variable ξ is updated using Eq. (13), where the current values of the variables appearing in the integrand are used. The semi-inverse iteration procedure is illustrated in Fig. 2.

Numerical Examples

The foregoing inviscid/viscid interaction analysis has been applied to several cascade configurations, two of which are discussed herein: a compressor exit guide vane (EGV) and a high-speed compressor (HSC) cascade. Blade surface and wake pressure coefficient, $C_P = (P - P_{-\infty})/2$, and displacement thickness δ distributions and blade surface shear stress, $\tau_w = Re^{-1}\, \mu \partial u/\partial n\,|_{n=0}$, distributions will be presented as functions of chordwise distance x for both cascades, where $x = 0$ and 1 at the leading and trailing edges, respectively. The IVI solutions will be evaluated through comparisons with Navier-Stokes solutions. In addition, the predicted values of the total pressure loss and the exit flow angle will be presented for the EGV cascade; these were obtained using the mixing analysis of Stewart.[19] Finally, the performance of the SFLOW-IVI analysis, i.e., its efficiency and convergence properties, will also be discussed.

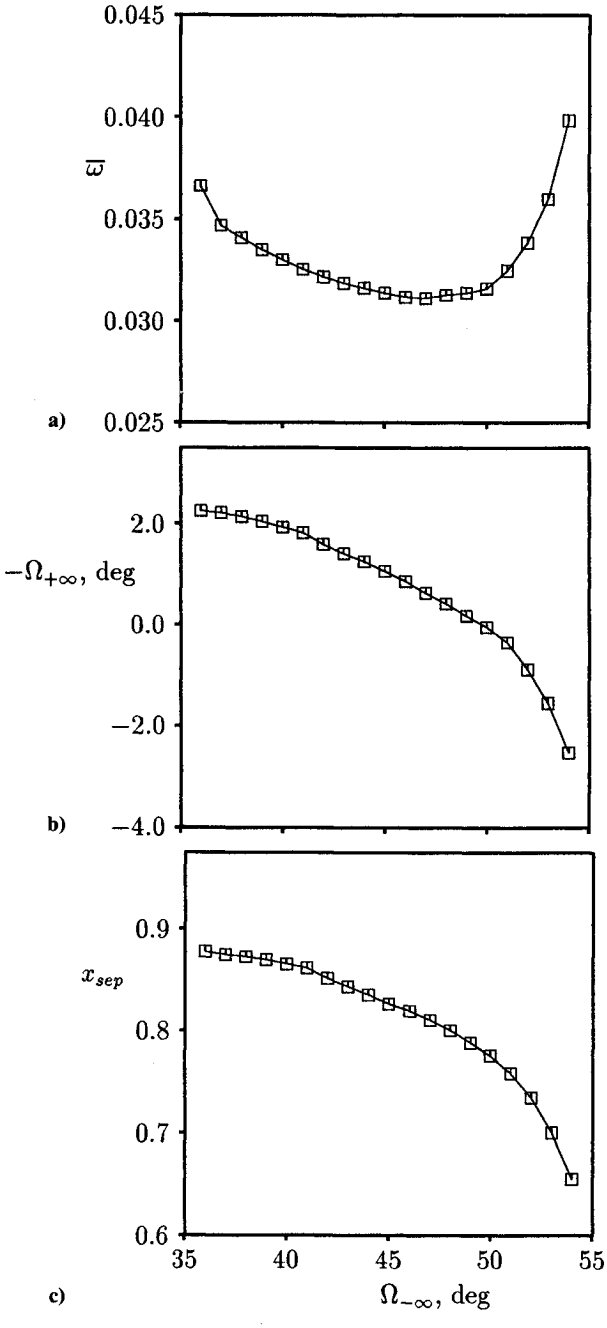

Fig. 6 Predictions for the EGV cascade for a range of inlet flow angles: a) loss parameter, b) exit flow angle, and c) separation point location.

In all of the calculations described here, the SFLOW-IVI analysis was applied using a convergence tolerance $\hat{\epsilon}$ of 0.001 [see Eq. (27)]. The inviscid meshes that were used for both cascades have the same dimensions, i.e., there are 90 axial and 31 circumferential lines, with 24 axial lines upstream of the leading edge, 41 lines intersecting the blade surfaces, and 25 lines aft of the trailing edge. The viscous-layer analysis employed a total of 81 blade and 25 wake streamwise grid lines, with 71 grid lines across the surface boundary layer and 141 grid lines across the wake. For the cases considered in this study, the wake curvature effect was assumed to be negligible; thus, $[\![P]\!]_W$ was set equal to zero, cf. Eq. (5). Although the wake curvature effect is formally of the same order of magnitude as the displacement interaction effect, our experience, based on estimates obtained from previous IVI solutions for geometries similar to those considered here, supports our assumption that the inclusion of this term has little impact on the final results.

Compressor Exit Guide Vane

The EGV cascade consists of 12% thick, highly cambered, modified NACA airfoils.[12] It has a stagger angle Θ of 15 deg and a gap-chord ratio G of 0.6, and it operates at a prescribed inlet Mach number $M_{-\infty}$ of 0.3 and an inlet flow angle $\Omega_{-\infty}$ of 40 deg. Calculations were performed for an inviscid flow and for viscous flows at Reynolds numbers of 10^5 and 10^6. In the latter, instantaneous transition from laminar to turbulent flow was assumed to occur at 1% of the arc distance measured from the leading-edge stagnation point to the trailing edge on both the suction and pressure surfaces of the blades. A streamline mesh is depicted in Fig. 3, where three adjacent EGV blade passages are shown. For the purpose of illustration, the mesh shown in this figure has approximately half the number of axial and circumferential grid lines than were used for the actual calculations.

Results of the inviscid and IVI calculations are given in Fig. 4. The blade and wake pressure and displacement thickness distributions are shown in Figs. 4a and 4b, respectively, and the surface shear-stress distributions along the blade are shown in Fig. 4c. The expected approach of the viscous to the inviscid solution as Re is increased is evident in Fig. 4a. The rate of growth of the suction-surface displacement thickness increases with increasing x as the trailing edge is approached. As shown in Fig. 4c, a suction-surface separation bubble ($\tau_w < 0$) exists and spans approximately 14% of chord at $Re = 10^6$ and about 24% of chord for $Re = 10^5$. The decrease in the extent of the separation bubble as Re is increased is consistent with the behavior expected for turbulent flows.

The surface pressure, displacement thickness, and shear-stress distributions predicted by SFLOW-IVI are compared in Fig. 5 with results obtained using the Navier-Stokes analysis of Dorney et al.[20] for the $Re = 10^6$ case. This analysis uses the Baldwin-Lomax turbulence model,[21] which is very similar to the Cebeci-Smith model used in SFLOW-IVI. Good agreement between the results of the two procedures is obtained over most of the blade surface. However, the agreement deteriorates in the vicinity of the trailing edge, which is most likely caused by the use of an O-mesh around the blades in the Navier-Stokes analysis. The O-mesh topology is not well suited for flows over thin trailing-edge geometries because it produces mesh lines that are severely skewed in the vicinity of the trailing edge. This skewing introduces inaccuracies into the numerical solution. In addition, the integral appearing in the definition of δ [see Eq. (11)] should be evaluated along lines that are normal to the body surface. However, near the trailing edge, the integration is carried out along skewed O-mesh lines, which deviate significantly from the surface normal direction, producing questionable results for the local δ distribution. Both analyses predict separation ($\tau_w < 0$) from the suction surface and give almost identical predictions for the location of the separation point ($\tau_w = 0$; see Fig. 5c).

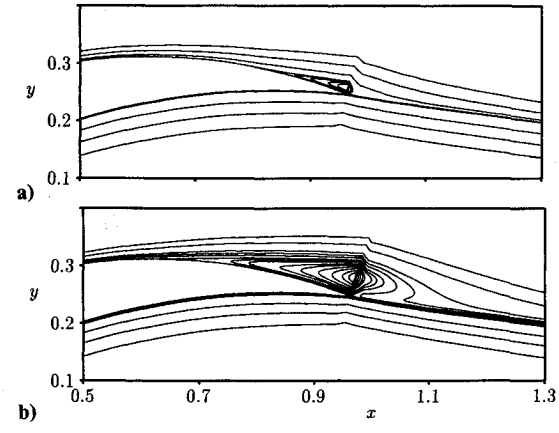

Fig. 7 Trailing-edge streamline patterns for the EGV cascade: a) $\Omega_{-\infty} = 45$ deg and b) $\Omega_{-\infty} = 54$ deg.

To test the robustness of the SFLOW-IVI analysis, additional calculations were carried out for $M_{-\infty}=0.3$, $Re = 10^6$, and a wide range of inlet flow angles, $36 \leq \Omega_{-\infty} \leq 54$ deg. The transition point locations were held fixed at $s/s_{TE} = 0.01$ for all values of $\Omega_{-\infty}$. This location is the same as that reported earlier for the baseline calculation ($\Omega_{-\infty}=40$ deg). The results are shown in Fig. 6, where the predicted total pressure loss parameter, $\bar{\omega} = (P_{t-\infty} - P_{t+\infty})/(P_{t-\infty} - P_{-\infty})$ (where P_t is the total pressure), exit flow angle $\Omega_{+\infty}$, and separation point location at $x = x_{sep}$ are plotted as functions of $\Omega_{-\infty}$. Solutions could not be obtained for $\Omega_{-\infty} < 36$ deg because a small supersonic region, which could not be treated using the present version of SFLOW-IVI, formed near the blade leading edge. At $\Omega_{-\infty} = 54$ deg, the viscous layer is approaching stall, with the separation region spanning approximately 35% of chord. Above 54 deg the solution would not converge due to a numerical instability. This is consistent with the stability properties of the semi-inverse IVI iteration procedure when applied to flows with large-scale separations.[22]

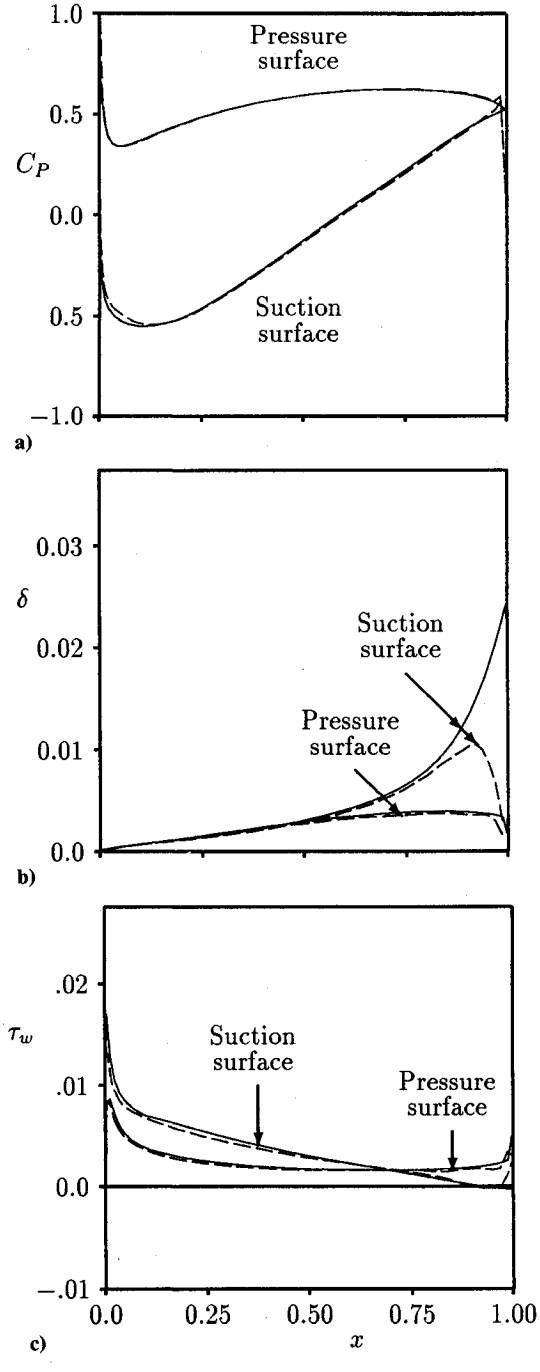

Fig. 8 Comparison of IVI (——) and Navier-Stokes (- - - - -) solutions for the HSC cascade at $Re = 10^6$: a) pressure coefficient, b) displacement thickness, and c) surface shear stress.

The total pressure loss parameter and the exit flow angle are plotted vs $\Omega_{-\infty}$ in Figs. 6a and 6b, respectively. There is a wide range of inlet flow angles over which the loss remains relatively low, but $\bar{\omega}$ increases rapidly as the inlet flow angle is increased above 50 deg. The latter corresponds to the rapid inflation of the separation region with increasing $\Omega_{-\infty}$ for $\Omega_{-\infty} > 50$ deg, which can be seen in Fig. 6c. A striking similarity exists between the variations in $-\Omega_{+\infty}$ and x_{sep} as $\Omega_{-\infty}$ is varied, as is apparent from comparing the results shown in Figs. 6b and 6c. The streamwise growth of the separation bubble as $\Omega_{-\infty}$ is increased is accompanied by a similar increase in the suction-surface displacement thickness in the vicinity of the trailing edge. This produces a thickened displacement body (i.e., blade plus displacement thickness), reducing the effective camber of the blade and thus the loading it produces. As a direct consequence there is a reduction in the turning of the flow, i.e., an increase in $\Omega_{+\infty}$.

The predicted streamline patterns indicating the size of the trailing-edge separation bubble for $\Omega_{-\infty} = 45$ and 54 deg are shown in Fig. 7. For $36 \leq \Omega_{-\infty} \leq 45$ deg the separation bubble grows slowly, whereas much more rapid growth occurs between 45 and 54 deg (see Fig. 6c). The decambering effect produced by the growth of the separation bubble is clearly illustrated by the results in Fig. 7. The kinks that appear in the streamlines near the trailing edge require some explanation. Since the blade trailing edge is wedge shaped, the surface coordinate line formed by the blade surface and reference wake streamline has a geometric singularity or "kink" at the trailing edge. This singularity influences the solution throughout the trailing-edge region as shown in the streamline plots in Fig. 7. Because this singular behavior is highly localized, its effect on the overall flowfield solution is negligible.

High-Speed Compressor

The HSC cascade consists of cambered NACA 0006 airfoils.[12] This cascade operates at high-subsonic inlet conditions, i.e., $M_{-\infty} = 0.7$ and $\Omega_{-\infty} = 55$ deg, and has a blade spacing and a stagger angle of unity and 45 deg, respectively.

Inviscid and viscous calculations were performed for the HSC cascade operating at $Re = 10^5$ and 10^6, producing behavior similar to that observed for the EGV cascade. The surface pressure coefficient, displacement thickness, and shear-stress distributions obtained for $Re = 10^6$ using SFLOW-IVI are compared in Fig. 8 with those obtained using the Navier-Stokes analysis of Ref. 20. The agreement is excellent except in the immediate vicinity of the trailing edge. The two analyses give almost identical predictions for the location of the separation point. Again, the differences in the two solutions are attributed to the use of an O-mesh, for thin trailing-edge profiles, in the Navier-Stokes analysis.

Timing Study and Convergence Behavior

Because the development of an efficient analysis has been a major objective of this analytical effort, a timing study was conducted for the cascade configurations examined herein. This provides both a measure of the computational effort currently required to obtain solutions using SFLOW-IVI and benchmarks against which future efforts to improve efficiency can be compared. The results are summarized in Table 1. In addition to the CPU time t_c, the relaxation factor ω, and the number of global iterations N_g required to converge the solution using a tolerance level $\hat{\epsilon}$ of 0.001 are given in Table 1. The execution times were determined using the nearly optimal value of ω obtained by trial and error.

The calculations were carried out on an HP-Apollo 720 workstation where SFLOW-IVI has been compiled using an optimizing preprocessor. No attempt has been made to "tune" the code to take advantage of special features of the optimizer. The times given in Table 1 are CPU times for the

Table 1 Summary of SFLOW-IVI CPU times t_C for different cascade configurations

Configuration	ω	N_g	t_C, s
EGV, $Re = 10^6$	1.20	24	197
EGV, $Re = 10^5$	0.85	38	277
HSC, $Re = 10^6$	1.20	27	203
HSC, $Re = 10^5$	0.80	40	296

portion of the calculation associated with the IVI iteration loop. Any overhead associated with initialization of the data structure, generation of the mesh, and calculation of the initial inviscid solution is not included. However, this overhead amounts to a small percentage of the overall CPU time required by the present analysis. Note that each of the solutions was obtained in less than 5 min.

It is difficult to make direct comparisons with Navier-Stokes CPU times since these can vary considerably, even by orders of magnitude, depending on numerous factors, including whether the code is a research or a design code, the number of grid points, the grid stretching, the convergence tolerance, and so on. An estimate based on a Navier-Stokes analysis that is currently used in design indicates that the present IVI analysis requires one to two orders of magnitude less CPU time to produce similar results.

The convergence behavior of two parameters of interest to compressor blade designers was examined to determine if a different measure of convergence than that given by Eq. (27) would be more appropriate for engineering applications. For the two compressor cascades, the total pressure loss parameter $\bar{\omega}$ and exit flow angle $\Omega_{+\infty}$ were monitored during the IVI iterations. We have found that the values of $\bar{\omega}$ and $\Omega_{+\infty}$ could be considered converged at a significantly lower iteration count than was needed to satisfy the convergence criterion ($\hat{\epsilon} = 0.001$); typically about one-third fewer iterations than are shown in Table 1 are needed. Thus, even greater efficiency could be achieved in many cases by measuring convergence by the degree to which the parameters of interest have approached their "asymptotic" values.

Concluding Remarks

Existing nonlinear inviscid and inverse viscous-layer analyses have been extended and coupled to provide a strong inviscid/viscid interaction analysis (SFLOW-IVI) for two-dimensional, subsonic, cascade flows. This analysis can be used to predict the effects of local strong interactions, including trailing-edge/near-wake interactions and viscous-layer separations, on cascade performance. The SFLOW-IVI analysis has proven to be both efficient and robust. Converged solutions for each of the baseline configurations examined herein were obtained in less than 5 min on an HP-Apollo 720 workstation. Even lower CPU times can be obtained by basing convergence on the global quantities of interest to an engine designer. Robustness was demonstrated via application to a wide range of inlet flow conditions, including conditions leading to separation bubbles extending up to 35% of blade chord.

A number of issues still need to be addressed to improve the accuracy of the present analysis and to expand its range of applicability. Among them are the inclusion of transonic and quasi-three-dimensional (i.e., stream tube contraction and radius change) effects and the incorporation of models for determining the transition from laminar to turbulent flow. In addition, the overall utility of the SFLOW-IVI analysis for design system applications needs to be explored through further testing and validation. Finally, as this effort continues, the focus will increasingly turn toward the development of a strong inviscid/viscid interaction capability for unsteady flows.

Acknowledgments

This research was supported by NASA Lewis Research Center under Contract NAS3-25425, with George Stefko serving as NASA program monitor. The authors are indebted to D. Hoyniak, NASA Lewis, for providing the SFLOW inviscid analysis and for helping with the modifications to that code, and D. J. Dorney, United Technologies Research Center, for his assistance in obtaining the Navier-Stokes solutions.

References

[1]Melnik, R. E., "Turbulent Interactions on Airfoils at Transonic Speeds—Recent Developments," AGARD-CP-291, Feb. 1981, Chap. 10.

[2]Lock, R. C., and Firmin, M. C. P., "Survey of Techniques for Estimating Viscous Effects in External Aerodynamics," Royal Aircraft Establishment, TM Aero 1900, Farnborough, England, UK, April 1981.

[3]Girodroux-Lavigne, P., and Le Balleur, J. C., "Unsteady Viscous-Inviscid Interaction Method and Computation of Buffeting over Airfoils," ONERA TP 1987-58, April 1987.

[4]Howlett, J. T., "Calculation of Viscous Effects on Transonic Flow for Oscillating Airfoils and Comparisons with Experiment," NASA TP 2731, Sept. 1987.

[5]Barnett, M., and Verdon, J. M., "Viscid/Inviscid Interaction Analysis of Subsonic Turbulent Trailing-Edge Flows," *AIAA Journal,* Vol. 25, No. 9, 1987, pp. 1184–1193.

[6]Veldman, A. E. P., "The Calculation of Incompressible Boundary Layers with Strong Viscous-Inviscid Interaction," AGARD-CP-291, Feb. 1981, Chap. 12.

[7]Janssens, P., and Hirsch, C., "A Viscid Inviscid Interaction Procedure for Two-Dimensional Cascades," AGARD-CP-351, Sept. 1983, Chap. 3.

[8]Calvert, W. J., and Herbert, M. V., "An Inviscid-Viscous Interaction Method to Predict the Blade-to-Blade Performance of Axial Compressors," *Aeronautical Quarterly,* Vol. XXXI, Pt. 3, 1980, pp. 173–196.

[9]Barnett, M., Hobbs, D. E., and Edwards, D. E., "Inviscid-Viscous Interaction Analysis of Compressor Cascade Performance," *ASME Journal of Turbomachinery,* Vol. 113, No. 4, 1991, pp. 538–553.

[10]Hoyniak, D., and Verdon, J. M., "Development of a Steady Potential Solver for Use with Linearized, Unsteady Aerodynamic Analyses," NASA TM 105288, Sept. 1991.

[11]Hoyniak, D., personal communication, Oct. 1991.

[12]Verdon, J. M., and Hall, K. C., "Development of a Linearized Unsteady Aerodynamic Analysis for Cascade Gust Response Predictions," NASA CR 4308, July 1990.

[13]Cebeci, T., and Smith, A. M. O., *Analysis of Turbulent Boundary Layers,* Academic Press, New York, 1974, Chap. 6.

[14]Chang, K. C., Bui, M. N., Cebeci, T., and Whitelaw, J. H., "The Calculation of Turbulent Wakes," *AIAA Journal,* Vol. 24, No. 2, 1986, pp. 200, 201.

[15]Blottner, F. G., "Finite Difference Method of Solution of the Boundary-Layer Equations," *AIAA Journal,* Vol. 18, No. 2, 1970, pp. 193–205.

[16]Vatsa, V. N., Werle, M. J., and Verdon, J. M., "Viscid/Inviscid Interaction at Laminar and Turbulent Symmetric Trailing Edges," AIAA Paper 82-0165, Jan. 1982.

[17]Barnett, M., Verdon, J. M., and Ayer, T. C., "Development of an Analysis for High Reynolds Number Inviscid/Viscid Interactions in Cascades," NASA Contractor Rept. 4519, May 1993.

[18]Carter, J. E., "A New Boundary Layer Inviscid Iteration Technique for Separated Flow," AIAA Paper 78-1450, July 1978.

[19]Stewart, W. L., "Analysis of Two-Dimensional Compressible Flow Loss Characteristics Downstream of Turbomachine Blade Rows in Terms of Basic Boundary-Layer Characteristics," NACA TN 3515, July 1955.

[20]Dorney, D. J., Davis, R. L., and Edwards, D. E., "Investigation of Hot Streak Migration and Film Cooling Effects on Heat Transfer in Rotor/Stator Interacting Flows," United Technologies Research Center, UTRC Rept. 91-29, East Hartford, CT, April 1992 (prepared under NAVAIR Contract N00140-88-C-0677).

[21]Baldwin, B. S., and Lomax, H., "Thin-Layer Approximation and Algebraic Model for Separated Turbulent Flows," AIAA Paper 78-257, Jan. 1978

[22]Wigton, L. B., and Holt, M., "Viscous-Inviscid Interaction in Transonic Flow," AIAA Paper 81-1003, June 1981.